JSLHR

Research Article

Intravelar and Extravelar Portions of Soft Palate Muscles in Velic Constrictions: A Three-Dimensional Modeling Study

Peter Anderson,[a] Sidney Fels,[a] Ian Stavness,[b] William G. Pearson, Jr.,[c] and Bryan Gick[d,e]

Purpose: This study predicts and simulates the function and relative contributions of the intravelar and extravelar portions of the levator veli palatini (LVP) and palatoglossus (PG) muscles in velic constrictions.
Method: A finite element-based model of the 3-dimensional upper airway structures (palate, pharynx, tongue, jaw, maxilla) was implemented, with LVP and PG divided into intravelar and extravelar portions. Simulations were run to investigate the contributions of these muscles in velopharyngeal port (VPP) closure and constriction of the oropharyngeal isthmus (OPI).
Results: Simulations reveal that the extravelar portion of LVP, though crucial for lifting the palate, is not sufficient to effect VPP closure. Specifically, the characteristic "bulge" appearing in the posterior soft palate during VPP closure (Pigott, 1969; Serrurier & Badin, 2008) is found to result from activation of the intravelar portion of LVP. Likewise, the intravelar portion of posterior PG is crucial in bending the "veil" or "traverse" (Gick, Francis, Klenin, Mizrahi, & Tom, 2013) of the velum anteriorly to produce uvular constrictions of the OPI (Gick et al., 2014).
Conclusions: Simulations support the view that intravelar LVP and PG play significant roles in VPP and OPI constrictions.

The soft palate is essential in speech, swallowing, and breathing, yet our understanding remains incomplete as to the relative contributions of the intrinsic and extrinsic portions of the muscles most central to soft palate control. Descriptions of the actions of the soft palate focus on two muscles in particular: levator veli palatini (LVP), described as constricting the velopharyngeal port (VPP) by raising the soft palate, and palatoglossus (PG), described as contributing to constriction of the oropharyngeal isthmus (OPI) by lowering the soft palate (e.g., Fritzell, 1969). LVP and PG both contain portions that are external and internal to the soft palate (Cho, Kim, Lee, & Yoon, 2013; Kuehn & Azzam, 1978; Perry, Kuehn, & Sutton, 2013; Perry, Kuehn, Sutton, & Gamage, 2014). Perry et al. (2013), following the terminology of Huang, Lee, and Rajendran (1997a), describe the extravelar portion of LVP as the segment extending from the origin to the insertion point into the velum and the intravelar portion as the length of the entire muscle segment contained within the velum. This article applies this distinction to both LVP and PG, presenting a three-dimensional (3D) biomechanical model of the soft palate that focuses on the distinct roles that the intravelar and extravelar portions of LVP and PG play in controlling the VPP and OPI.

The extravelar and intravelar portions of LVP and PG exhibit markedly different structures, positions, and fiber directions. Although the extravelar portions of both muscles are comparatively thick and linear, the intravelar portions are more fanned out and interdigitated with other muscles, making the latter challenging to measure accurately using electromyography (Kuehn, Folkins, & Cutting, 1982) and thus less subject to previous study. A diagram of the oral and pharyngeal regions is provided in Figure 1, highlighting the approximate location and muscle fiber direction of the extravelar portions of LVP and PG muscles. Consistent with these fiber directions, experimental measurements correlate palatal raising with LVP activation (Fritzell, 1969) and palatal lowering with PG activation (Fritzell, 1969; Lubker, 1968; Lubker, Fritzell, & Lindqvist, 1970).

[a]Department of Electrical and Computer Engineering, University of British Columbia, Vancouver, Canada
[b]Department of Computer Science, University of Saskatchewan, Saskatoon, Canada
[c]Department of Cellular Biology and Anatomy, Medical College of Georgia, Georgia Regents University, Augusta
[d]Department of Linguistics, University of British Columbia, Vancouver, Canada
[e]Haskins Laboratories, New Haven, CT
Correspondence to Bryan Gick: gick@mail.ubc.ca

Editor-in-Chief: Julie Liss
Editor: Monica McHenry
Received October 31, 2017
Revision received April 13, 2018
Accepted November 6, 2018
https://doi.org/10.1044/2018_JSLHR-S-17-0247

Disclosure: *The authors have declared that no competing interests existed at the time of publication.*

Figure 1. A diagram of the upper airway with key components labeled and fiber directions of the extravelar portions of LVP and PG illustrated (adapted from image by Patrick J. Lynch, medical illustrator [CC BY 2.5, http://creativecommons.org/licenses/by/2.5], via Wikimedia Commons).

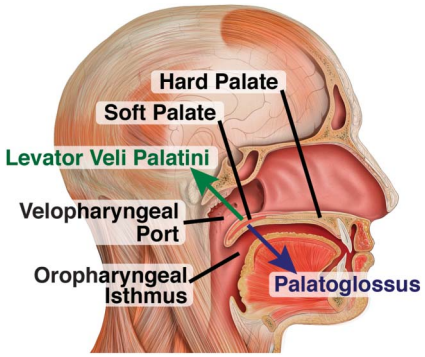

Though some early follow-up studies raised doubts that PG was involved in palatal lowering (Bell-Berti, 1976; Bell-Berti & Hirose, 1973; Berti & Hirose, 1971), it was later clarified that PG can indeed be involved in active lowering of the soft palate but that not all languages and contexts employ active lowering (Benguerel, Hirose, Sawashima, & Ushijima, 1977; Dixit, Bell-Berti, & Harris, 1987).

Based on the fiber directions of the extrinsic portions of LVP and PG, one might expect VPP closure and OPI constriction to be in conflict with one another (e.g., Seaver & Kuehn, 1980). That is, one might expect the LVP activation to close the VPP to be directly antagonistic with the PG activation to constrict the OPI. Kuehn et al. (1982) describe some antagonism between LVP and PG (as well as palatopharyngeus), suggesting that this may be mitigated somewhat by the elasticity of the palate and will vary based on palate and tongue position. However, Gick et al. (2013) show that speakers producing the French uvular can constrict the OPI using active motion of the posterior palate toward the tongue without compromising VPP closure. This observation that both VPP and OPI may function independently brings into question the antagonism between VPP and OPI function and challenges the representation of the soft palate as a simple "trapdoor" (Biavati, Sie, Wiet, & Rocha-Warley, 2009) that is pulled up or down to close the VPP or OPI under extravelar muscle force. We suggest that the intravelar portions of LVP and PG may be essential to VPP and OPI constriction.

One long-standing point of interest regarding the function of intravelar muscles has been the formation of the "midline bulge" or "levator eminence" (Huang, Lee, & Rajendran, 1997b) or "velar eminence" (Perry et al., 2013). Pigott (1969) provided an early report of this midline convexity on the nasopharyngeal surface of the soft palate during speech. Serrurier and Badin (2008) provide a detailed 3D reconstruction of the soft palate clearly showing this bulge forming in the central posterior region of the soft palate as part of VPP closure. The muscular mechanism underlying the midline bulge has been the subject of some discussion, often involving musculus uvulae. According to Boorman and Sommerlad (1985), "It has been widely suggested that musculus uvulae is responsible for this nasal convexity of the palate seen during speech." Although Azzam and Kuehn (1977) agree regarding the importance of musculus uvulae in forming the bulge, both they and Boorman and Sommerlad also cite the importance of LVP, a position echoed by Huang et al. (1997b). We aim to clarify the role of LVP in producing the midline bulge, with a particular focus on the relative contributions of the intravelar and extravelar portions, by simulating the actions of these muscles using computational biomechanical modeling.

A number of previous computational models have simulated the soft palate, generally focusing on LVP and its contribution to VPP closure. Two-dimensional (2D) models have represented the soft palate as a 2D beam with muscle descriptions, with VPP closure driven by extravelar muscle forces (Berry, Moon, & Kuehn, 1999), or have based model VPP closure on a 2D model of the palate and surrounding structures in the plane of LVP (Srodon, Miquel, & Birch, 2012). Moving away from a strictly midsagittal representation of the soft palate, a 3D yet beamlike palate model (Inouye, Pelland, Lin, Borowitz, & Blemker, 2015) demonstrates VPP closure that agrees with Kuehn and Moon's (1998) experimental data despite lacking palate–pharynx connectivity. A 3D, spring–mass representation of the palate (Inouye, Perry, Lin, & Blemker, 2015) provides an insightful model showing the consequence of anatomical or muscle variations on VPP closure.

Gick et al. (2014), using a 3D palate model but without a model of the pharynx, show that the intravelar portion of PG is necessary for OPI constriction. Given that the fiber direction of intravelar portions of LVP and PG is largely perpendicular to the midsagittal plane, focusing on the role of these intravelar portions necessitates a comprehensive 3D description of the soft palate and its muscles. To do this, we extend a previously reported upper airway model to include muscle-driven finite element (FE) soft palate and pharynx models (Anderson, Harandi, Moisik, Stavness, & Fels, 2015). The model's morphology is consistent with the previous model, but the soft palate has been remeshed to be of finer resolution and composed predominantly of hexahedral elements in order to improve the fidelity of soft palate deformations. Although the previous study focused on tongue muscle activations to generate different vocal tract shapes, here, we focus on soft palate and pharyngeal muscle activations in order to simulate VPP closure and OPI constriction.

A 3D computational model provides the freedom of treating the intravelar and extravelar portions of LVP and PG as functionally independent, even if they are not. We do this to highlight the role that the intravelar portion plays and to reveal the contributions that are neglected by a unitary representation. In this study, we seek to elucidate whether the intravelar portions produce a significant

effect and, if so, whether the intravelar and extravelar portions serve functions that are synergistic, independent, or even opposed. Though other muscles are involved in VPP and OPI constriction, we focus on LVP and PG because they appear to be antagonistic muscles whose primary functions govern VPP and OPI constriction, and previous observations suggest a more complicated relationship between them, likely involving the unexamined intravelar portions.

This study thus aims to describe the roles of the intravelar portions of LVP and PG and how those roles relate to the functional targets of VPP and OPI constriction. The following sections present a computational model in detail, presenting simulations of VPP constriction highlighting the contributions of intravelar and extravelar portions of LVP, as well as simulations of OPI constriction while maintaining VPP closure.

Method

Our model is defined and simulated using the ArtiSynth biomechanical simulation toolkit (Lloyd, Stavness, & Fels, 2012). ArtiSynth can simulate the dynamics of composite models that include coupled soft tissue (FE models) and hard tissue (rigid body models) components, together with skin meshes that deform along with the neighboring components to which they are attached. The upper airway model used in this study (see Figures 2, 3, and 5) is an aggregate model of multiple, previously published source components (see Table 1). Two subjects were used to generate the morphology of the source components. Cone beam computed tomography data for Subject S1 (male, 35 years old, Caucasian) were segmented to obtain 3D surfaces for the skull, jaw, and hyoid bone and inner surface of the pharynx. Magnetic resonance imaging (MRI) data for Subject S2 (male, 40 years old, Caucasian) were segmented to obtain 3D surfaces for the face, tongue, soft palate, and laryngeal structures. Surface segmentations were performed manually using Amira (Thermo Fisher Scientific). The reliability of manual segmentations was enhanced by choosing the best modality to image each structure (hard tissues with cone beam computed tomography, soft tissues with MRI, and tissue–air boundaries with either modality). Muscle attachments and fiber directions were arranged in putative locations and guided by MRI data where possible. All components were coregistered to the MRI data for S2 using the mesh-match-and-repair (MMRep) algorithm (Bucki, Nazari, & Payan, 2010). Additional details regarding model construction have been published elsewhere (see Anderson et al., 2017). Here, we provide additional details for the soft palate and pharynx components, which are of primary interest to this study.

Figure 2. A midsagittal view of the biomechanical model providing an overview of the upper airway components included in the computational model. The yellow line indicates the location of the cross-section used to calculate closure areas.

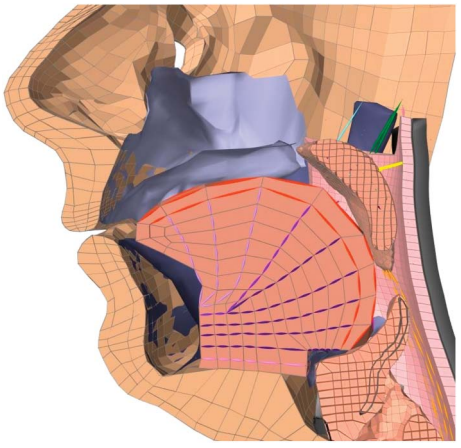

Soft Palate

The soft palate, shown in Figure 3, was meshed using a hexahedral dominant mesh. The soft palate material is based on the description of Birch and Srodon (2009), who divide the soft palate into 10 zones, each with a measured value of Young's modulus (E) and the ratio of glandular to muscle tissue in that zone. Based on these values, we divided the stiffness into glandular and muscular components with best fit values of E_{muscle} = 1,776 Pa and $E_{\text{glandular}}$ = 516 Pa. Based on the rounded $E_{\text{glandular}}$ value, we model the soft palate using a linear elastic material with E = 500 Pa. The embedded point-to-point muscles have a passive force to approximate the E_{muscle} contribution to the overall stiffness of the soft palate. We use a constant Poisson ratio of v = 0.4995, but note that this may vary throughout the soft palate (Birch & Srodon, 2009).

Soft palate muscle paths were fit to the palate and pharynx geometries informed by anatomical descriptions of the soft palate (Cho et al., 2013; Drake, Vogl, & Mitchell, 2010; Kuehn & Kahane, 1990). Muscles are represented as point-to-point Hill-type muscles, following the muscle model of Peck, Langenbach, and Hannam (2000). The active force that a muscle can produce is a function of its length, as shown in Figure 4, which is scaled by the muscle's activation level. However, the muscles also produce a passive force that is present even when the muscle is not activated, which is also shown in Figure 4. Muscle fibers were either embedded within an FE model, connected to a rigid body, or anchored to a fixed point in space. The soft palate muscles, including their abbreviated names and maximum forces, are summarized in Table 2. Reported cross-sectional areas (CSAs) of the LVP (Perry et al., 2013) and PG (Cho et al., 2013) are used to define the maximum muscle force based on the relationship $F_{\text{max}} = A_{\text{cs}} \cdot K$, where A_{cs} is the CSA of the muscle and K is the specific tension of muscle tissue, a constant usually assigned the value of K = 40 N/cm^2 (Peck et al., 2000). The other muscles (tensor veli palatini, palatopharyngeus, and musculus uvulae), which play an important passive role in these simulations, are assigned an approximate value of 3 N for F_{max}.

Figure 3. Front (left) and sagittal (right) views of the soft palate and pharynx models. Half of the palate is rendered semitransparent to show internal muscle fibers, including the levator veli palatini (green), anterior palatoglossus (magenta), posterior palatoglossus (dark magenta), tensor veli palatini (cyan), palatopharyngeus (orange), and musculus uvulae (purple).

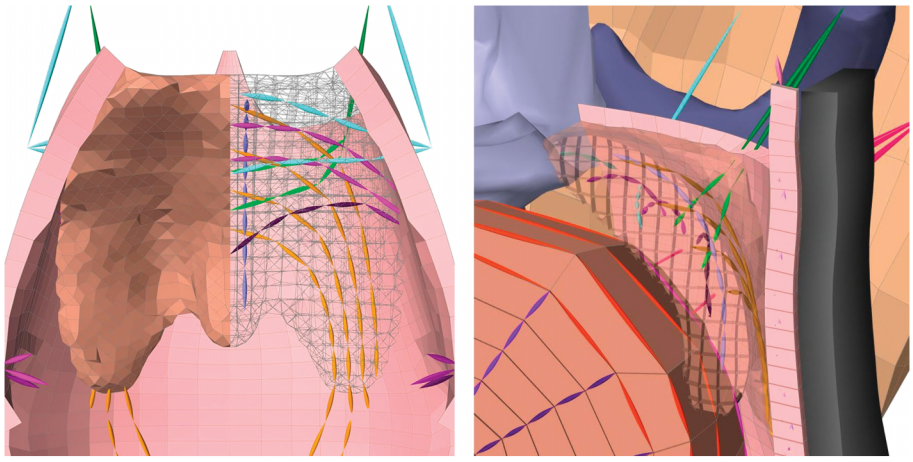

Table 3 provides comparisons between the LVP dimensions of our model and those reported in previous studies by Perry et al. (2013). The lengths are calculated as the average length of the two parallel fibers; extravelar length was measured from origin to insertion in palate, and intravelar length was measured from insertion in palate to the midsagittal plane. The total LVP length is within the range reported by Perry et al. (2013), but our extravelar length is outside their range, suggesting that the cutoff between extravelar and intravelar in our model is different than theirs. The velum–LVP angle (the angle at the LVP midsagittal center between the LVP origin and the posterior nasal spine) is slightly outside 1 *SD* from that reported by Inouye, Perry, et al. (2015).

Pharynx

The geometry and muscles of the pharynx are shown in Figure 5. The basic pharynx geometry was derived by fitting spline surfaces to the pharyngeal constrictor muscles in computed tomography data, and the muscle paths were overlaid by a PhD in human anatomy. The spline surfaces were then approximated with a single smooth surface with a quadrangle mesh, and this mesh and the muscle paths were nonrigidly mapped to the upper airway model based on landmarks of other upper airway components. Finally, the quadrangle mesh was extruded to form a hexahedral mesh 2.9 mm thick superiorly and 4.0 mm thick inferiorly (Anderson et al., 2015). The pharynx is modeled as a linear material having E = 15,000 Pa and v = 0.49.

Superiorly, the exterior nodes belonging to the top row of elements in the narrow portion of the pharynx are fixed, approximating attachment to the skull. Inferiorly, the exterior nodes belonging to the bottom elements are fixed, approximating attachment to inferior cartilaginous structures and esophagus. The exterior nodes along the midsagittal centerline are treated as fixed, but a rigid component was added posterior to the pharynx to act as a

Table 1. Summary of components included in upper airway simulation.

Component	Type	Complexity	Reference
Face	FE	8,720 nodes	Nazari et al. (2010)
Tongue	FE	948 nodes	Buchaillard et al. (2009)
Soft palate	FE	3,081 nodes	Chen et al. (2012), Gick et al. (2014)
Pharynx	FE	2,436 nodes	Anderson et al. (2017)
Larynx	FE	3,034 nodes	Moisik & Gick (2013)
Skull, jaw, hyoid	Rigid	6 *df* (×3)	Stavness et al. (2011)
Larynx cartilage	Rigid	6 *df* (×7)	Moisik & Gick (2013)
Simple spine	Rigid	6 *df*	N/A
Nasal airway	Skin	N/A	Stavness et al. (2014)

Note. The table includes component name, component type (either FE models, rigid body, or deformable skin surface), component complexity (number of nodes for FE models and degrees of freedom [*df*] for rigid structures), and references to source publications. FE = finite element; N/A = not applicable.

Figure 4. The model describing the passive and active force generation capabilities of soft palate muscles.

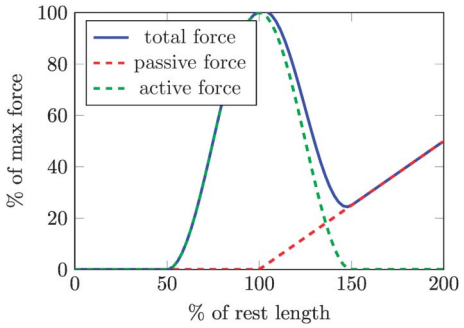

simple spine model that constrains posterior motion of the pharynx (the dark gray component visible in Figure 2). The pharynx is also attached to the tongue, soft palate, and laryngeal structures at locations of muscle insertion. Although the fixed inferior and posterior attachments of the pharynx model are more restrictive than their real attachments would be, all attachments local to the phenomena under investigation are appropriate, with the lateral pharyngeal walls free to deform and thus constitute an integral part of the simulations.

Simulation Procedures

A skin mesh, representing the inner surface of the nasal airway passage above the soft palate, and its centerline were added to monitor the CSA and closure force of the VPP at 10 locations at evenly spaced increments along the velopharynx. Kuehn and Moon (1998), whose experiments provide a means of validation, measured the closure force at a location of maximal force using a force bulb approximately 5 mm in radius. Following this protocol, we sum the collision forces within a 5-mm radius of each of the 10 locations monitored. The third most superior location proved generally to be the location of minimal CSA and maximal closure force and is the location reported in the remainder of this study. This area is shown in yellow in Figure 2.

The face and larynx, which are isolated from the movements being simulated, are treated as nondynamic to save computation effort but still serve as attachment points for the surrounding structures.

Table 2. Muscle groupings used in this study.

Muscle name	Short name	Max force (N)
Levator veli palatini	LVP	10.8
Palatoglossus (anterior)	PGA	2.1
Palatoglossus (posterior)	PGP	1.1
Tensor veli palatini	TVP	3
Palatopharyngeus	PP	3
Musculus uvulae	MU	3

The simulation of contact between the soft palate and pharynx causes spurious forces that may appear/oscillate for a few time steps. Therefore, we filter the force response function first using a median filter with a width of nine samples and then calculate the moving average over a width of 0.08 s.

We consider three sequences of muscle activations in this study.

1. LVP alone is activated, demonstrating the resulting VPP CSA and force response.
2. LVP is split into extravelar and intravelar portions, which are activated sequentially to distinguish the roles of intravelar and extravelar musculature.
3. After VPP closure is achieved using LVP, the PG is activated to observe the role of intravelar and extravelar portions in constricting the OPI.

Results

We now present our results, first demonstrating VPP closure as the result of intravelar and extravelar portions of LVP and second showing how the quality of OPI constriction depends on PG activation strategies.

VPP Closure

The VPP closure behavior of the model using LVP alone is illustrated in Figure 6, for which both intravelar and extravelar portions of LVP are gradually activated simultaneously from 0 to 1 (see Figure 6, top), and the resulting area functions (see Figure 6, middle) and force functions (see Figure 6, bottom) are displayed. These results show that VPP CSA drops to less than 0.5 cm^2 by approximately 0.2 s following LVP activation, which is consistent with previously reported aerodynamic data (Dalston, Warren, & Smith, 1990). Although $E = 500$ Pa is the default Young's modulus, Figure 6 also displays the area and force response for E being two times and 10 times our default value to show the consequences of stiffening the palate. These higher stiffnesses are within the range used by other studies (Cheng, Gandevia, Green, Sinkus, & Bilston, 2011; Inouye, Pelland, et al., 2015; Inouye, Perry, et al., 2015).

From Figure 6, we observe that the VPP achieves nearly complete closure by $t = 0.4$ s, which corresponds to approximately 30% activation. The area never drops all the way to zero due to small off-midline gaps and numerical artifacts in the CSA calculation. The closure forces attain maximum values before the activation reaches 100%. This unexpected behavior most likely occurs after portions of the palate have risen above the margins of the pharynx and thus above the region where palate–pharynx forces are calculated. The length of LVP (extravelar and intravelar portions on one side) at 100% activation is 25.9 mm, which is 61.7% of the rest length (42.0 mm). Based on the muscle model, shown in Figure 4, we would not expect a muscle to contract below 50% of the rest length,

Table 3. Comparison of levator veli palatini (LVP) dimensions to those reported in past studies.

Muscle name	This study	Reported value
LVP len (mm)	42.0	41.7–52.9 (Perry et al., 2013)
LVP extrapalatal len (mm)	25.4	26.8–34.7 (Perry et al., 2013)
LVP intrapalatal len (mm)	16.6	14.0–20.0 (Perry et al., 2013)
Velum–LVP angle (degrees)	85.7	78.5 ± 5.23 *SD*s (Inouye, Perry, et al., 2015)

and already at 61.7% rest length, the muscle is only able to produce about 20% of its maximum force.

We also consider the case where the extravelar and intravelar portions of LVP are activated sequentially, as illustrated in Figure 7 (top). The area response (see Figure 7, middle) shows that extravelar LVP alone achieves two thirds of the VPP closure, yet only after the intravelar portion of LVP is activated does the VPP form complete closure. The force plot (see Figure 7, bottom) shows that activation of the intravelar portion of LVP generates more than 90% of the total closure force between the palate and pharyngeal wall. Again, we see a distinctive maximal force around $t = 0.6$ s, which is likely a transient feature of the palate–pharynx collision.

The anatomical response to this LVP activation sequence is shown in Figure 8. One can observe that activation of extravelar LVP alone appears to create near-closure midsagitally but clearly fails to achieve closure off midline (see Figure 8, middle). Only after the intravelar portion of LVP activates does the soft palate form a firm closure against the pharyngeal wall (see Figure 8, bottom). Figure 9 illustrates the shape of the palate before and after LVP is activated. As Figure 9 (right) shows, activation of LVP produces a midline bulge similar in form to that shown by Serrurier and Badin (2008).

OPI Constriction

Having examined the quality of VPP closure as produced by intravelar and extravelar LVP, we turn our attention to independent constriction of the OPI after VPP closure. VPP closure is achieved between $0 < t < 0.2$ s by activating LVP to 30%, shown in the previous section to cause adequate closure both in terms of CSA and force.

Figure 5. Posterior oblique views of the model with the pharynx rendered semitransparent to show internal muscle fibers, including the superior constrictor (green), middle constrictor (magenta), inferior constrictor (purple), cricopharyngeus (red), salpingopharyngeus (cyan), stylopharyngeus (yellow), and palatopharyngeus (orange, left image).

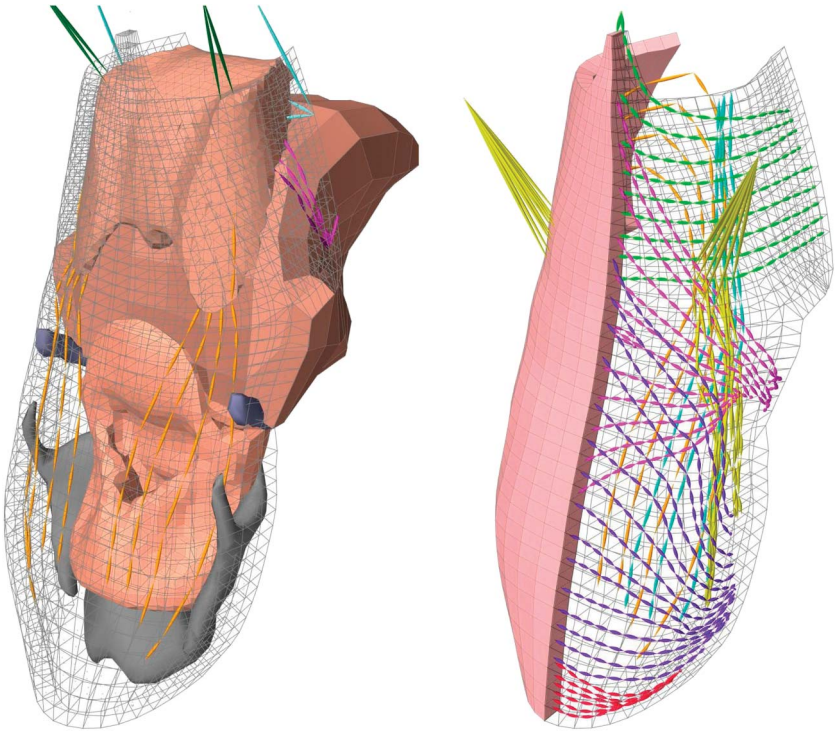

Figure 6. Muscle activations (top), velopharyngeal cross-sectional area (middle), and closure force (bottom) versus time for different stiffnesses of the soft palate under concurrent activation of extravelar (ext) and intravelar (int) levator veli palatini. This simulation reveals the rapid reduction of velopharyngeal cross-sectional area with levator veli palatini activation and the stronger closure force of a stiffer soft palate.

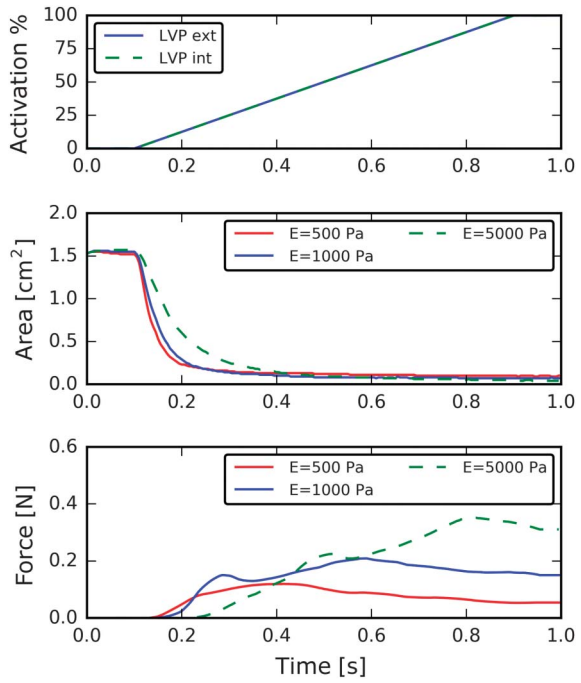

Figure 7. Muscle activations (top), velopharyngeal cross-sectional area (middle), and closure force (bottom) versus time for sequential activations of extravelar (ext) and intravelar (int) levator veli palatini (LVP). This simulation reveals that, although extravelar LVP alone contributes to the majority of velopharyngeal port closure, the intravelar portion of LVP is required for complete closure.

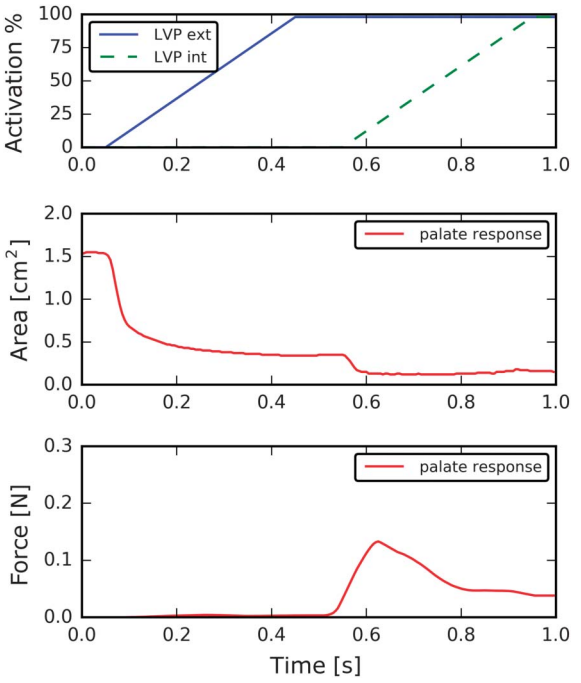

From $0.2 < t < 0.6$ s, no new activations are introduced, given the model time to reach steady state, and then at $t = 0.6$ s, PG starts to activate (see Figure 10, starts at $t = 0.55$ s to focus on the change caused by PG activation). We consider activation of PG as a whole, activation of only posterior PG (PGP), and activation of only the intravelar or extravelar portion of PGP. Figure 10 shows that activating PG as a whole increases the CSA of VPP closure and diminishes VPP closure force. However, activating only the intravelar PGP leads to no appreciable loss of closure area or force. Included in Figure 10 is the motion measured by the tip of the uvula. Here, we observe that intravelar PGP, although not compromising VPP closure force, causes the largest motion of the uvula, with 25% more motion than PGP and 36% more uvular motion than PG as a whole. In contrast, activation of PG or PGP causes similar motion of the uvula yet compromises VPP closure.

Figure 11 shows the anatomical consequences of PG activation, which are plotted in Figure 10. As compared with the VPP closure without any PG activation (see Figure 11b), activation of PG (see Figure 11c), PGP (see Figure 11d), and intravelar PGP (see Figure 11f) causes similar uvula motion, bending the uvula anteriorly toward the tongue and thereby contributing to OPI constriction (see Gick et al., 2013). However, activation of PG causes noticeable deformation to other portions of the palate, and PG and PGP are shown to compromise the quality of VPP closure (see Figure 10), though not readily visible in Figures 11c and 11d. The extrinsic PGP (see Figure 11e) does not cause anterior uvula motion similar to Figures 11c, 11d, and 11f.

To visualize the action of PGP, a simulation was run in which only PGP was activated to 30%. This is illustrated in Figure 12, in a view comparable to Figure 3 (left). One can see a bulge form around the course of PGP rather than a distinctive palatoglossal arch. This suggests that either the PG muscle may be too deeply embedded or the palate material may be too stiff in that region.

Discussion

This study reveals that the intravelar portions of LVP and PG play central roles in soft palate function for VPP and OPI constriction. Intravelar LVP is largely responsible for producing the midline bulge observed in the posterior region of the soft palate during VPP closure (Pigott, 1969; Serrurier & Badin, 2008) and is responsible for more than 90% of VPP closure force while maintaining a constant activation of musculus uvulae. Although previous studies have generally recognized VPP as being largely responsible for VPP closure, none have suggested such a dominant role

Figure 8. Midsagittal cutaway (left) and transverse cutaway (right) views of the model at rest (top) with extravelar levator veli palatini (LVP) activation (middle) and with extravelar and intravelar LVP activation (bottom). With extravelar LVP activation, the velopharyngeal port appears closed midsagittally, but the transverse view reveals that the closure is not complete off the midsagittal plane (middle). Additional activation of intravelar LVP results in complete velopharyngeal port closure (bottom).

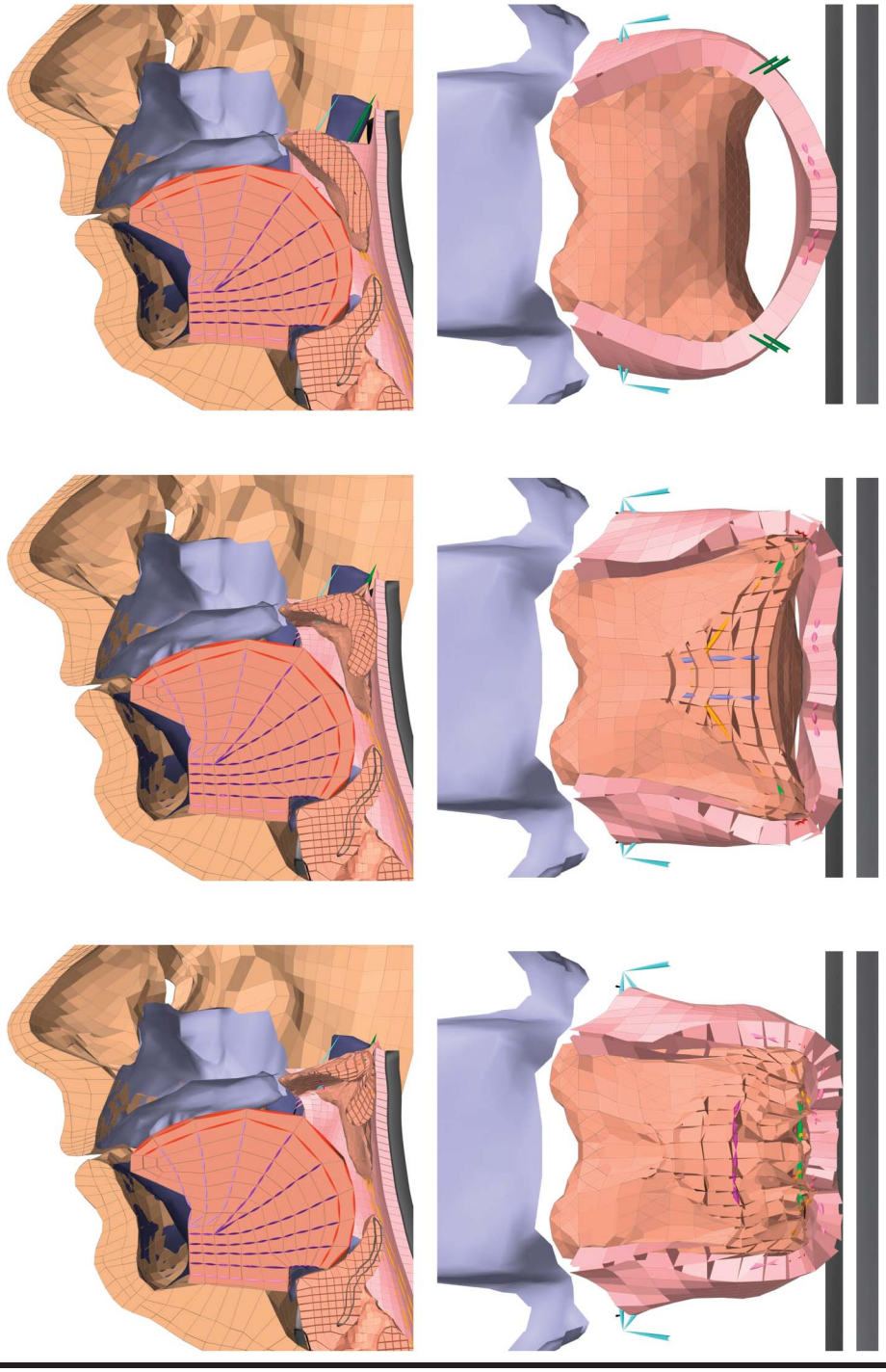

for the intravelar portion. Likewise, intravelar PG is shown to provide important control of the OPI constriction with minimal impact on the quality of VPP closure. The unique and significant roles of these intravelar portions indicate a shortcoming of the trapdoor representation of the soft palate, which places VPP and OPI control in opposition (see Seaver & Kuehn, 1980). Not only are these roles observed to be important, but they are also demonstrated to

Figure 9. Oblique posterior view of the soft palate at rest (left) and with 50% levator veli palatini activation, illustrating the bulge formed as a result of levator veli palatini activation (right).

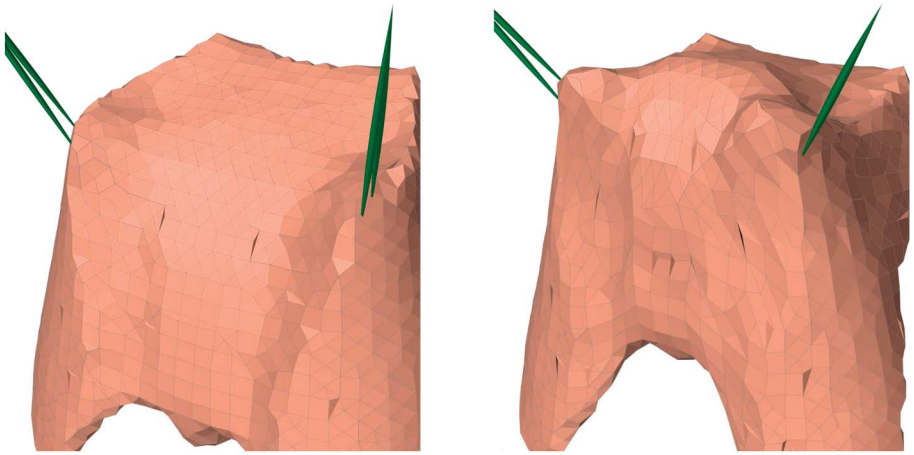

serve functional goals that complement their extravelar counterparts. Hence, even if the intravelar and extravelar portions could be activated independently, they would be functionally motivated to coactivate. Both the intravelar and extravelar portions of LVP and PG are observed to contribute distinctly and significantly toward their common functional goals of constricting the VPP and OPI (respectively).

Figure 10. Muscle activations (a), velopharyngeal cross-sectional area (b), closure force (c), and anterior uvula movement (d) versus time for sequential activation of levator veli palatini (LVP) and palatoglossus (PG). First, (a) LVP is activated to create velopharyngeal port (VPP) closure, followed by PG; the portions of PG that are activated affect the VPP closure as illustrated by (b) the resulting VPP area function, (c) the resulting VPP closure forces, and (d) the distance moved anteriorly by the uvula. The intravelar posterior PG (PGP) has little effect on VPP area or closure force but results in the largest uvula motion. Dist = distance; ext = extravelar; int = intravelar.

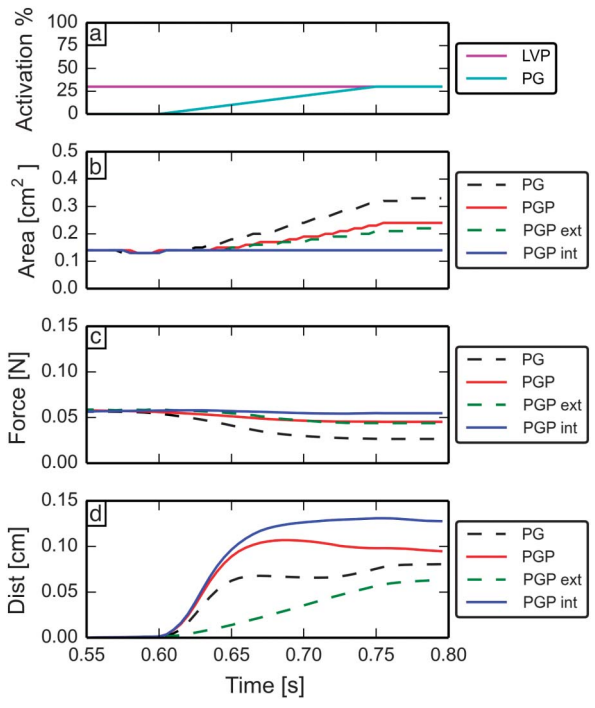

A model that accounts for the biomechanics of the LVP and PG could be useful in addressing velopharyngeal insufficiency, resulting from abnormal development, cancer treatment, or iatrogenic causes. A recent 3D FE model of VPP closure compared different scenarios of cleft palate repair (Inouye, Pelland, et al., 2015). Although that model uses 3D FE analysis, the model morphology is not fully 3D with a flat posterior pharyngeal wall, allowing that model to achieve a complete VPP closure with 0.6-N closure force with extravelar LVP activation alone; this does not accurately represent LVP muscle function in VPP closure to aid in surgical planning to repair cleft palates or short soft palates. Our model represents the 3D concave mediolateral curvature of the posterior pharyngeal wall. This more realistic 3D morphology highlights the role of intravelar LVP muscles in contouring the soft palate to conform to the concave shape of the pharynx. More anatomically and biomechanically accurate models are more likely to provide useful outcomes compared to more simplified models. Examples of such applications include surgical treatment of oral or nasopharyngeal cancers, which often impacts the palate (Siddiqi & Connor, 2013) and which could benefit from modeling outcomes of new approaches to surgical oblation of cancerous tissue. A common treatment for velopharyngeal insufficiency is autologous fat injection pharyngoplasty (Leuchter, Schweizer, Hohlfeld, & Pasche, 2010), in which the present model could be used to test various injection sites and volumes to improve outcomes.

Kuehn and Azzam (1978), in a dissection study, observe that, in most specimens, PG attaches more toward the uvula than the hard palate, such that it is situated so as to have a mechanical advantage in lowering the soft palate. However, PG does attach closer to the hard palate

Figure 11. Midsagittal view of the model, showing the oropharyngeal isthmus and velopharyngeal port (VPP) consequences of activating portions of palatoglossus (PG). Arrows indicate motion due to PG. Model shown at rest (a), with levator veli palatini activated alone (b), with PG activated (c), with posterior PG (PGP) activated (d), with extravelar PGP activated (e), and with intravelar PGP activated (f). After VPP closure is achieved with levator veli palatini (b), activating PG (c) or only PGP (d) results in anterior uvula motion but also diminishes VPP closure quality (see Figure 10). Extravelar PGP alone produces no noticeable uvula motion (e), but intravelar PGP produces uvula motion with little compromise of VPP closure quality.

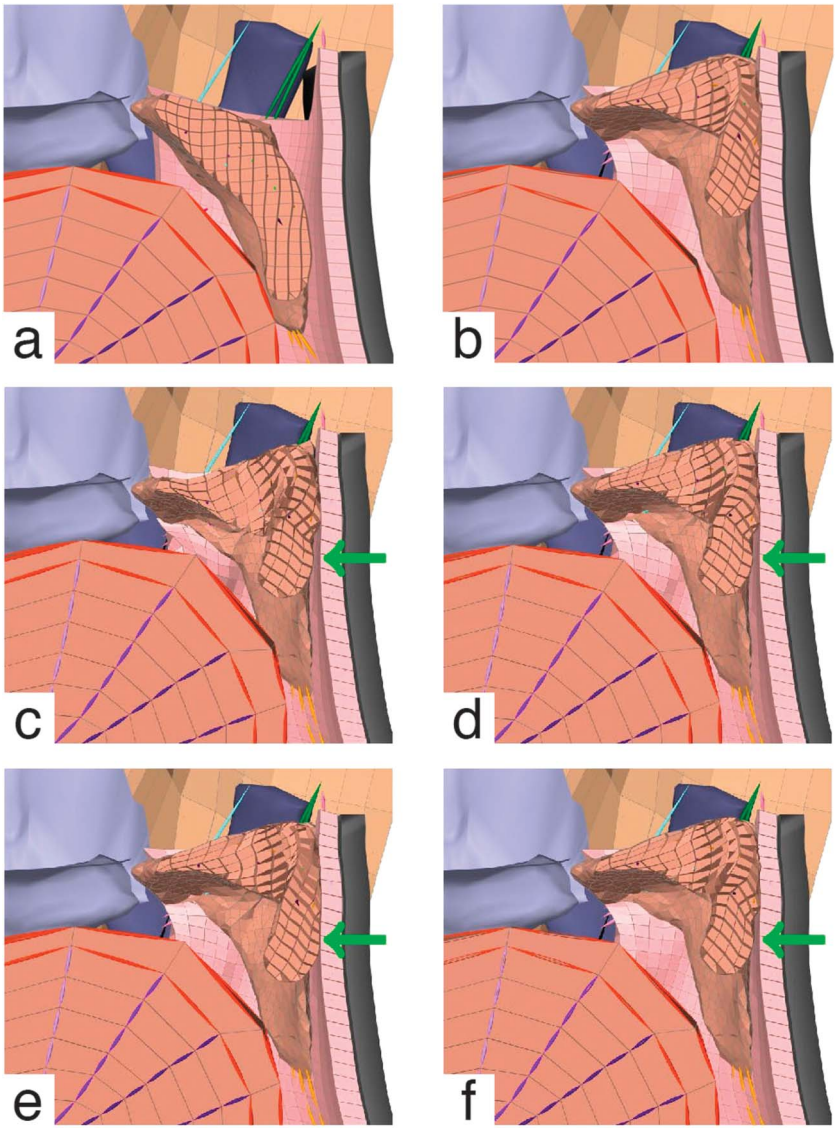

in some specimens, suggesting that it may be mechanically advantaged for raising the tongue rather than lowering the palate. In the present model, PG is fanned out, so that anterior PG is closer to the hard palate whereas PGP is closer to the uvula. The effectiveness of PGP in constricting the OPI by bending the uvula anteriorly toward the tongue (see Gick et al., 2013), particularly with minimal compromise to VPP closure, suggests a further advantage that a more PGP has in controlling the motion of the soft palate (see also Gick et al., 2014).

Although previous imaging studies have provided measures of the intravelar and extravelar portions at least for LVP (Perry et al., 2013, 2014), it is difficult to fully determine their functional properties without observing their actions in isolation. In this respect, computational modeling of the kind presented here becomes an essential tool in uncovering function. This article has elucidated the vital and distinct roles played by the intravelar portions of LVP and PG, as well as how the intravelar and extravelar portions of both muscles work together

Figure 12. Front view of the oral cavity at rest (left) and after posterior palatoglossus is activated (right). The anterior faucial pillars enlarge after posterior palatoglossus activation but are not distinctive, suggesting a shortcoming in the design of the current model.

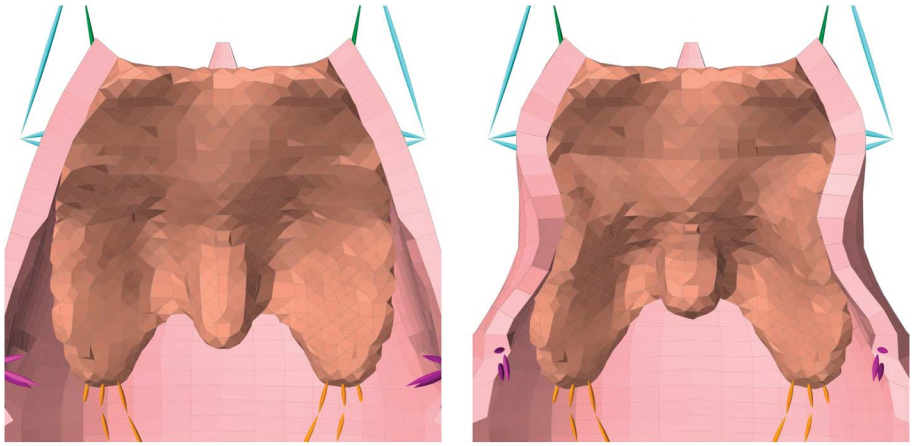

toward the common functional goals of VPP and OPI constriction.

Limitations

This study only examined the LVP and PG muscles for the sake of highlighting the role of the intravelar portions of those muscles. However, other muscles are known to be involved in VPP closure and OPI constriction (e.g., Kuehn et al., 1982); thus, this study does not attempt to provide a complete picture of VPP and OPI control. The tissue and muscle geometries used in our model were derived from medical images and published literature with reference to standard anatomy and hence are expected to be plausible. However, they were not derived from a single subject, which is a possible drawback to our model.

The trends predicted by these simulations provide insight into the function of the soft palate musculature; however, the magnitude of the closure force and the distance moved by the uvula are points of concern. The magnitude of the closure force is sensitive to Young's modulus (see Figure 6), but we also observed sensitivity to how compressibility is handled. In these simulations, compressibility is not strictly enforced. In the cases where we do strictly enforce compressibility, the closure forces are near the magnitude of those reported by Kuehn and Moon (1998), but the soft palate becomes unnaturally stiff and bulky. Modeling the viscoelastic behavior of the soft palate was not deemed essential given that the primary concern of this study was with the final (time-independent) postures resulting from muscle activations. However, it would be more appropriate to model the soft palate with viscoelastic parameters (Birch & Srodon, 2009). Such modifications to the material properties would likely improve the resultant VPP closure response forces, though we do not anticipate it changing the observed trends.

For some velic postures, the faucial pillars stand out prominently, suggesting that palatopharyngeus and PG muscles are shallowly embedded in very soft tissue. In our simulations, the faucial pillars do not stand out with such prominence (see Figure 12), particularly the anterior pillars (arising from PG), which suggests that PG may be too stiffly embedded in the soft palate model. This restriction of the PG muscle is likely to be an important factor toward the relatively small anterior motion of the uvula during the OPI constriction gesture.

Conclusions

We have presented a 3D FE model of the soft palate that is part of a complete upper airway model. In these simulations, the soft palate is driven by muscle activations of LVP and PG (though all palatal muscles are present in the model and provide passive forces). Simulations with this model demonstrate closure of the VPP and anterior flexion of the uvula in the OPI without compromising velopharyngeal closure. The model identifies the importance of intravelar LVP musculature for producing more than 90% of the VPP closure force and replicating the posterior shape observed experimentally by Serrurier and Badin (2008). The model also identifies the independent activation of intravelar portions of PG in order to maximize oropharyngeal articulation without compromising velopharyngeal closure.

This study demonstrates that intravelar soft palate musculature is necessary for the soft palate to achieve the versatility that it is observed to have and is required to have for speech production. More generally, the study provides an example of the value of biomechanical simulation for isolating the functions of distinct portions of muscles. In this respect, this study adds to a growing literature describing functionally distinct divisions of oral muscles, including genioglossus (Dang & Honda, 2002),

styloglossus and hyoglossus (Honda, Murano, Takano, Masaki, & Dang, 2013), and superior longitudinalis (Stone, Epstein, & Iskarous, 2004).

Acknowledgments

The authors are very grateful to the Natural Sciences and Engineering Research Council (Grant CHRP 414167-12), the National Institutes of Health (Grant DC-002717 to Haskins Laboratories), and the Canadian Institutes of Health Research (Grant CPG-121024) for providing funding for this research.

References

Anderson, P., Fels, S., Harandi, N. M., Ho, A., Moisik, S., Sánchez, C. A., . . . Tang, K. (2017). Chapter 20 FRANK: A hybrid 3D biomechanical model of the head and neck. In Y. Payan & J. Ohayon (Eds.), *Biomechanics of living organs* (pp. 413–447). Oxford, United Kingdom: Academic Press.

Anderson, P., Harandi, N. M., Moisik, S., Stavness, I., & Fels, S. (2015). A comprehensive 3D biomechanically-driven vocal tract model including inverse dynamics for speech research. In *Interspeech 2015,* Dresden, Germany.

Azzam, N., & Kuehn, D. (1977). The morphology of the musculus uvulae. *The Cleft Palate Journal, 14,* 79–87.

Bell-Berti, F. (1976). An electromyographic study of velopharyngeal function in speech. *Journal of Speech and Hearing Research, 19*(2), 225–240.

Bell-Berti, F., & Hirose, H. (1973). Patterns of palatoglossus activity and their implications for speech organization. *The Journal of the Acoustical Society of America, 54*(1), 320.

Benguerel, A., Hirose, H., Sawashima, M., & Ushijima, T. (1977). Velar coarticulation in French: An electromyographic study. *Journal of Phonetics, 5,* 157–167.

Berry, D., Moon, J., & Kuehn, D. (1999). A finite element model of the soft palate. *Cleft Palate–Craniofacial Journal, 36,* 217–223.

Berti, F., & Hirose, H. (1971). Velopharyngeal function in oral/nasal articulation and voicing gestures. *Haskins Laboratory Status Report on Speech Research, 28,* 143–156.

Biavati, M. J., Sie, K., Wiet, G. J., & Rocha-Worley, G. (2009). Velopharyngeal insufficiency. *eMedicine: Otolaryngology and Facial Plastic Surgery,* 1–21.

Birch, M. J., & Srodon, P. D. (2009). Biomechanical properties of the human soft palate. *Cleft Palate–Craniofacial Journal, 46,* 268–274.

Boorman, J., & Sommerlad, B. (1985). Musculus uvulae and levator palati: Their anatomical and functional relationship in velopharyngeal closure. *British Journal of Plastic Surgery, 38,* 333–338.

Buchaillard, S., Perrier, P., & Payan, Y. (2009). A biomechanical model of cardinal vowel production: Muscle activations and the impact of gravity on tongue positioning. *The Journal of the Acoustical Society of America, 126,* 2033–2051.

Bucki, M., Nazari, M. A., & Payan, Y. (2010). Finite element speaker-specific face model generation for the study of speech production. *Computer Methods in Biomechanics and Biomedical Engineering, 13,* 459–467.

Chen, H., Fels, S., Pang, T., Tsou, L., de Almeida, F. R., & Lowe, A. A. (2012). Three-dimensional reconstruction of soft palate modeling from subject-specific magnetic resonance imaging data. *Sleep and Breathing, 16,* 1113–1119.

Cheng, S., Gandevia, S., Green, M., Sinkus, R., & Bilston, L. (2011). Viscoelastic properties of the tongue and soft palate using MR elastography. *Journal of Biomechanics, 44,* 450–454.

Cho, J. H., Kim, J. K., Lee, H.-Y., & Yoon, J.-H. (2013). Surgical anatomy of human soft palate. *Laryngoscope, 123,* 2900–2904.

Dalston, R. M., Warren, D. W., & Smith, L. R. (1990). The aerodynamic characteristics of speech produced by normal speakers and cleft palate speakers with adequate velopharyngeal function. *The Cleft Palate Journal, 27*(4), 393–401.

Dang, J., & Honda, K. (2002). Estimation of vocal tract shapes from speech sounds with a physiological articulatory model. *Journal of Phonetics, 30*(3), 511–532.

Dixit, R., Bell-Berti, F., & Harris, K. (1987). Palatoglossus activity during nasal/nonnasal vowels of Hindi. *Phonetica, 44*(4), 210–226.

Drake, R., Vogl, A. W., & Mitchell, A. W. M. (2010). *Gray's anatomy for students* (2nd ed.). Philadelphia, PA: Churchhill Livingstone.

Fritzell, B. (1969). The velopharyngeal muscles in speech. An electromyographic and cineradiographic study. *Acta Oto-Laryngologica,* Suppl. 250:1+.

Gick, B., Anderson, P., Chen, H., Chiu, C., Kwon, H. B., Stavness, I., . . . Fels, S. (2014). Speech function of the oropharyngeal isthmus: A modeling study. *Computer Methods in Biomechanics and Biomedical Engineering: Imaging & Visualization, 2,* 217–222.

Gick, B., Francis, N., Klenin, A., Mizrahi, E., & Tom, D. (2013). The velic traverse: An independent oral articulator? *The Journal of the Acoustical Society of America, 133,* 208–213.

Honda, K., Murano, E. Z., Takano, S., Masaki, S., & Dang, J. (2013). Anatomical considerations on the extrinsic tongue muscles for articulatory modeling. *Proceedings of Meetings on Acoustics, 19*(1). https://doi.org/10.1121/1.4800262

Huang, M. H., Lee, S. T., & Rajendran, K. A. (1997a). A fresh cadaveric study of the paratubal muscles: Implications for eustachian tube function in cleft palate. *Plastic and Reconstructive Surgery, 100,* 833–842.

Huang, M. H., Lee, S. T., & Rajendran, K. A. (1997b). Structure of the musculus uvulae: Functional and surgical implications of an anatomic study. *Cleft Palate–Craniofacial Journal, 34*(6), 466–474.

Inouye, J. M., Pelland, C. M., Lin, K. Y., Borowitz, K. C., & Blemker, S. S. (2015). A computational model of velopharyngeal closure for simulating cleft palate repair. *Journal of Craniofacial Surgery, 26,* 658–662.

Inouye, J. M., Perry, J. L., Lin, K. Y., & Blemker, S. S. (2015). A computational model quantifies the effect of anatomical variability on velopharyngeal function. *Journal of Speech, Language, and Hearing Research, 58,* 1119–1133.

Kuehn, D., & Azzam, N. (1978). Anatomical characteristics of palatoglossus and anterior facial pillar. *The Cleft Palate Journal, 15*(4), 349–359.

Kuehn, D., Folkins, J., & Cutting, C. (1982). Relationships between muscle-activity and velar position. *The Cleft Palate Journal, 19*(1), 25–35.

Kuehn, D., & Kahane, J. (1990). Histologic-study of the normal human adult soft palate. *The Cleft Palate Journal, 27,* 26–35.

Kuehn, D., & Moon, J. (1998). Velopharyngeal closure force and levator veli palatini activation levels in varying phonetic contexts. *Journal of Speech, Language, and Hearing Research, 41,* 51–62.

Leuchter, I., Schweizer, V., Hohlfeld, J., & Pasche, P. (2010). Treatment of velopharyngeal insufficiency by autologous fat injection. *European Archives of Oto-Rhino-Laryngology, 267*(6), 977–983.

Lloyd, J. E., Stavness, I., & Fels, S. (2012). ArtiSynth: A fast interactive biomechanical modeling toolkit combining multibody and finite element simulation. In Y. Payan (Ed.), *Soft tissue biomechanical modeling for computer assisted surgery* (pp. 355–394). Berlin, Germany: Springer.

Lubker, J. (1968). An electromyographic-cinefluorographic investigation of velar function during normal speech production. *The Cleft Palate Journal, 5,* 1–18.

Lubker, J., Fritzell, B., & Lindqvist, J. (1970). Velopharyngeal function: An electromyographic study. *Speech Transmission Laboratory Quarterly Progress and Status Report, 11,* 9–20.

Moisik, S., & Gick, B. (2013). The quantal larynx revisited. *The Journal of the Acoustical Society of America, 133,* 3522.

Nazari, M. A., Perrier, P., Chabanas, M., & Payan, Y. (2010). Simulation of dynamic orofacial movements using a constitutive law varying with muscle activation. *Computer Methods in Biomechanics and Biomedical Engineering, 13,* 469–482.

Peck, C., Langenbach, G., & Hannam, A. (2000). Dynamic simulation of muscle and articular properties during human wide jaw opening. *Archives of Oral Biology, 45,* 963–982.

Perry, J. L., Kuehn, D. P., & Sutton, B. P. (2013). Morphology of the levator veli palatini muscle using magnetic resonance imaging. *Cleft Palate–Craniofacial Journal, 50*(1), 64–75.

Perry, J. L., Kuehn, D. P., Sutton, B. P., & Gamage, J. K. (2014). Sexual dimorphism of the levator veli palatini muscle: An imaging study. *Cleft Palate–Craniofacial Journal, 51*(5), 544–552.

Pigott, R. W. (1969). The nasoendoscopic appearance of the normal palatopharyngeal valve. *Plastic and Reconstructive Surgery, 43,* 19–24.

Seaver, E., & Kuehn, D. (1980). A cineradiographic and electromyographic investigation of velar positioning in nonnasal speech. *The Cleft Palate Journal, 17,* 381–388.

Serrurier, A., & Badin, P. (2008). A three-dimensional articulatory model of the velum and nasopharyngeal wall based on MRI and CT data. *The Journal of the Acoustical Society of America, 123,* 2335–2355.

Siddiqi, A., & Connor, S. E. (2013). Imaging of the pharynx and larynx. *Imaging, 22*(1), 91047403.

Srodon, P. D., Miquel, M. E., & Birch, M. J. (2012). Finite element analysis animated simulation of velopharyngeal closure. *Cleft Palate–Craniofacial Journal, 49,* 44–50.

Stavness, I., Lloyd, J. E., Payan, Y., & Fels, S. (2011). Coupled hard–soft tissue simulation with contact and constraints applied to jaw–tongue–hyoid dynamics. *International Journal For Numerical Methods In Biomedical Engineering, 27,* 367–390.

Stavness, I., Nazari, M., Flynn, C., Perrier, P., Payan, Y., Lloyd, J., & Fels, S. (2014). Coupled biomechanical modeling of the face, jaw, skull, tongue, and hyoid bone. In N. Magnenat-Thalmann, O. Ratib, & F. Choi (Eds.), *3D multiscale physiological human* (pp. 253–274). London, United Kingdom: Springer.

Stone, M., Epstein, M., & Iskarous, K. (2004). Functional segments in tongue movement. *Clinical Linguistics and Phonetics, 18*(6–8), 507–521.